Research Article

Kun-Qiong Li*

Multiple rogue wave solutions of a generalized (3+1)-dimensional variable-coefficient Kadomtsev–Petviashvili equation

https://doi.org/10.1515/phys-2022-0043
received February 08, 2022; accepted May 09, 2022

Abstract: Kadomtsev–Petviashvili equation is used for describing the long water wave and small amplitude surface wave with weak nonlinearity, weak dispersion, and weak perturbation in fluid mechanics. Based on the modified symbolic computation approach, the multiple rogue wave solutions of a generalized (3+1)-dimensional variable-coefficient Kadomtsev–Petviashvili equation are investigated. When the variable coefficient selects different functions, the dynamic properties of the derived solutions are displayed and analyzed by different three-dimensional graphics and contour graphics.

Keywords: modified symbolic computation approach, rogue wave, fluid mechanics, plasma physics

1 Introduction

With the development of the world economy, maritime safety has become an important research topic in the field of marine engineering. Strong nonlinear waves can cause nonlinear problems such as wave climbing and slamming of offshore structures, which bring great wave loads and are a huge threat to the safety of offshore structures [1]. A rogue wave is such a strong nonlinear extreme wave with remarkable characteristics such as extremely high wave height, prominent wave crest, concentrated energy, and large destructive power. The concept of rogue wave was first proposed by Draper [2] in 1965, and since then, the phenomenon of rogue waves and its influence on offshore structures have received extensive attention. People called the rogue wave "deep sea monster," describing it like a wall of water, appearing suddenly, and then quickly disappearing without a trace. Currently, it has been found that rogue wave widely exist in various sea areas of the world, which can appear in the deep sea and offshore sea, in stormy weather and general weather, but most of them are stormy weather. Therefore, the study of rogue wave is of great significance [3–5].

In this work, under investigation is a generalized (3+1)-dimensional variable-coefficient Kadomtsev–Petviashvili equation (vcKPe) [6]:

$$\theta_1 u_x^2 + \theta_1 u u_{xx} + \theta_2 u_{xxxx} + \theta_3 u_{xx} + \theta_4 u_{xz} + \theta_5 u_{yy} + \theta_6 u_{zz} + \theta_7 u_{xy} + u_{xt} = 0, \tag{1}$$

where $u = u(x, y, z, t)$. Eq. (1) represents the long water wave and small amplitude surface wave with weak nonlinearity, weak dispersion, and weak perturbation in fluid mechanics, as well as the electrostatic wave potential in plasma physics. $\theta_i = \theta_i(t)$ $(i = 1, 2, \ldots, 7)$ is arbitrary function, describing the nonlinearity, dispersion, perturbed effect, and disturbed wave velocity along the y-and z-directions, respectively. Jaradat *et al.* [6] obtained the multiple soliton solutions and singular multiple soliton solutions for Eq. (1). Xie *et al.* [7] investigated the soliton collision and Bäcklund transformation of Eq. (1). Chai *et al.* [8] and Yin *et al.* [9] studied the rouge wave solutions for Eq. (1). Chai *et al.* [10] discussed the fusion and fission phenomena of Eq. (1). Chen and Tian [11] given the Gramian solutions and soliton interactions of Eq. (1). Liu and Zhu [12] presented the lump-type, breather wave, and kink-solitary wave solutions for Eq. (1). However, the multiple rogue wave solutions have not been derived, which will become our main work.

This article is organized as follows. Section 2 gives the one-order rogue wave solution; Section 3 presents the three-order rogue wave solution; Section 4 derives the six-order rogue wave solution; Section 5 presents a conclusion.

* **Corresponding author: Kun-Qiong Li,** College of General Education, Chongqing Industry Polytechnic College 401120, Chongqing, China, e-mail: 2609119072@qq.com

2 One-order rogue wave solution

Under the assumption

$$\theta_1 = 6\theta_2, \quad \kappa = x + \eta z - \Theta(t), \\ u = 2[\ln\psi]_{\kappa\kappa}, \quad \psi = \psi(\kappa, y), \tag{2}$$

where η is real constant, $\Theta(t)$ is undetermined function. Eq. (1) becomes

$$\begin{aligned}
&\phi\theta_1[(2\psi_\kappa^3 - 3\psi\psi_{\kappa\kappa}\psi_\kappa + \psi^2\psi_{\kappa\kappa\kappa})^2 + (\psi_\kappa^2 - \psi\psi_{\kappa\kappa})[6\psi_\kappa^4 \\
&- 12\psi\psi_{\kappa\kappa}\psi_\kappa^2 + 4\psi^2\psi_{\kappa\kappa\kappa}\psi_\kappa + \psi^2(3\psi_{\kappa\kappa}^2 - \psi\psi_{\kappa\kappa\kappa\kappa})]] \\
&- \theta_2[120\psi_\kappa^6 - 360\psi\psi_{\kappa\kappa}\psi_\kappa^4 + 120\psi^2\psi_{\kappa\kappa\kappa}\psi_\kappa^3 \\
&- 30\psi^2(\psi\psi_{\kappa\kappa\kappa\kappa} - 9\psi_{\kappa\kappa}^2)\psi_\kappa^2 + 6\psi^3(\psi\psi_{\kappa\kappa\kappa\kappa\kappa} \\
&- 20\psi_{\kappa\kappa}\psi_{\kappa\kappa\kappa})\psi_\kappa + \psi^3[-30\psi_{\kappa\kappa}^3 + 5\psi(2\psi_{\kappa\kappa\kappa}^2 \\
&+ 3\psi_{\kappa\kappa}\psi_{\kappa\kappa\kappa\kappa}) - \psi^2\psi_{\kappa\kappa\kappa\kappa\kappa\kappa}]] \\
&+ [-6\psi_\kappa^4 + 12\psi\psi_{\kappa\kappa}\psi_\kappa^2 - 4\psi^2\psi_{\kappa\kappa\kappa}\psi_\kappa \\
&+ \psi^2(\psi\psi_{\kappa\kappa\kappa\kappa} - 3\psi_{\kappa\kappa}^2)]\psi^2(\theta_3 + \eta(\theta_4 + \eta\theta_6) - \Theta'(t)) \\
&+ \theta_5[(2\psi\psi_{\kappa\kappa} - 6\psi_\kappa^2)\psi_y^2 - 2\psi(\psi\psi_{\kappa\kappa y} - 4\psi_\kappa\psi_{\kappa y})\psi_y \\
&+ \psi[\psi_{yy}(2\psi_\kappa^2 - \psi\psi_{\kappa\kappa}) + \psi[\psi\psi_{\kappa\kappa yy} \\
&- 2(\psi_{\kappa y}^2 + \psi_\kappa\psi_{\kappa yy})]]]\psi^2 + \theta_7[\psi[6\psi_{\kappa y}\psi_\kappa^2 \\
&- 3\psi\psi_{\kappa\kappa y}\psi_\kappa + \psi(\psi\psi_{\kappa\kappa\kappa y} - 3\psi_{\kappa y}\psi_{\kappa\kappa})] \\
&- \psi_y(6\psi_\kappa^3 - 6\psi\psi_{\kappa\kappa}\psi_\kappa + \psi^2\psi_{\kappa\kappa\kappa})]\psi^2 = 0.
\end{aligned} \tag{3}$$

Based on the modified symbolic computation approach [13–15], we suppose that Eq. (3) has the following solution:

$$\psi = (\kappa - \rho)^2 + \varepsilon_1(y - \varrho)^2 + \varepsilon_0, \tag{4}$$

where ρ, ϱ, ε_0, and ε_1 are unknown constants. Substituting Eqs. (4) into (3), we obtain

$$\Theta(t) = \int [\theta_3 + \eta\theta_4 - \varepsilon_1\theta_5 + \eta^2\theta_6]\mathrm{d}t, \ \theta_7 = 0, \\ \theta_5 = -\frac{3\theta_2}{\varepsilon_0\varepsilon_1}. \tag{5}$$

Substituting Eqs. (4) and (5) into Eq. (2), the one-order rogue wave solution of Eq. (1) is written as follows:

$$u = \left[4\left[-\left[\int\left(\frac{3\theta_2}{\varepsilon_0} + \theta_3 + \eta(\theta_4 + \eta\theta_6)\right)\mathrm{d}t + \rho - x - \eta z\right]^2 \right. \\ \left. + \varepsilon_1(y - \varrho)^2 + \varepsilon_0\right]] / \\ \left[\left[\left[\int\left(\frac{3\theta_2}{\varepsilon_0} + \theta_3 + \eta(\theta_4 + \eta\theta_6)\right)\mathrm{d}t + \rho - x - \eta z\right]^2 + \varepsilon_1(y - \varrho)^2 + \varepsilon_0\right]^2\right]. \tag{6}$$

When $\theta_3 = \theta_4 = \theta_6 = \theta_2 = 1$, Eq. (6) represents a rogue wave, which is shown in Figure 1. When $\theta_3 = \theta_6 = \theta_2 = 1$, $\theta_4 = t$, Eq. (6) has two rogue waves, which is shown in Figure 2. When $\theta_2 = \theta_3 = 1$, $\theta_4 = \sin(2t)$, $\theta_6 = 3\cos t$, Eq. (6) shows a periodic-type rogue wave, which is shown in Figure 3.

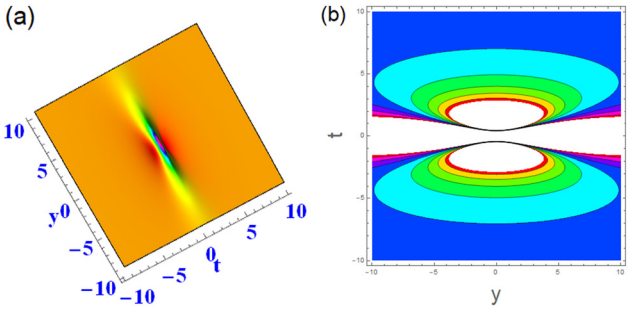

Figure 1: $\eta = -2$, $\varepsilon_0 = 3$, $\varepsilon_1 = 1$, $\rho = \varrho = x = z = 0$, (a) 3D plot and (b) contour plot.

3 Three-order rogue wave solution

To obtain the three-order rogue wave solution of Eq. (1), we choose

$$\begin{aligned}
\psi(\kappa, y) = &\rho^2 + \varrho^2 + \kappa^6 + y^6\varepsilon_{17} + y^4\varepsilon_{16} \\
&+ 2\rho\kappa(y^2\varepsilon_{23} + \kappa^2\varepsilon_{24} + \varepsilon_{22}) \\
&+ 2\varrho y(y^2\varepsilon_{20} + \kappa^2\varepsilon_{21} + \varepsilon_{19}) + \kappa^4 y^2\varepsilon_{11} + y^2\varepsilon_{15} \\
&+ \kappa^2(y^4\varepsilon_{14} + y^2\varepsilon_{13} + \varepsilon_{12}) + \kappa^4\varepsilon_{10} + \varepsilon_{18},
\end{aligned} \tag{7}$$

where ε_i $(i = 10, \ldots, 24)$ is unknown constant. Substituting Eq. (7) into Eq. (3), we derive

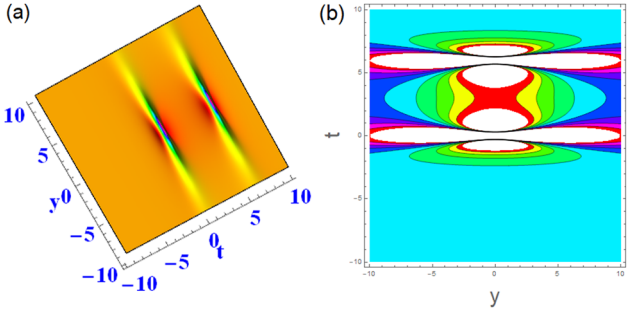

Figure 2: $\eta = -2$, $\varepsilon_0 = 3$, $\varepsilon_1 = 1$, $\rho = \varrho = x = z = 0$, (a) 3D plot and (b) contour plot.

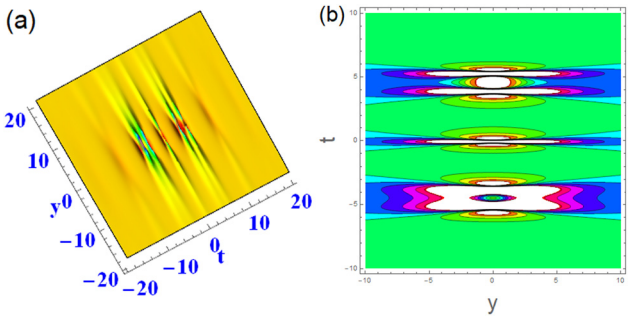

Figure 3: $\eta = -2, \varepsilon_0 = 3, \varepsilon_1 = 1, \rho = \varrho = x = z = 0$, (a) 3D plot and (b) contour plot.

$$
\begin{aligned}
&\varepsilon_{20} = -\frac{1}{9}\varepsilon_{11}\varepsilon_{21},\\
&\Theta(t) = \frac{\int (25\theta_2 + \varepsilon_{10}\theta_3 + \eta\varepsilon_{10}\theta_4 + \eta^2\varepsilon_{10}\theta_6)\mathrm{d}t}{\varepsilon_{10}},\\
&\theta_5 = -\frac{75\theta_2}{\varepsilon_{10}\varepsilon_{11}}, \varepsilon_{24} = -\frac{25\varepsilon_{22}}{\varepsilon_{10}}, \varepsilon_{14} = \frac{\varepsilon_{11}^2}{3},\\
&\varepsilon_{16} = \frac{17}{225}\varepsilon_{10}\varepsilon_{11}^2, \theta_7 = 0, \varepsilon_{17} = \frac{\varepsilon_{11}^3}{27}, \varepsilon_{15} = \frac{19}{75}\varepsilon_{10}^2\varepsilon_{11},\\
&\varepsilon_{13} = \frac{6\varepsilon_{10}\varepsilon_{11}}{5}, \varepsilon_{12} = -\frac{\varepsilon_{10}^2}{5}, \varepsilon_{19} = \frac{\varepsilon_{10}\varepsilon_{21}}{15}, \varepsilon_{23} = \frac{25\varepsilon_{11}\varepsilon_{22}}{\varepsilon_{10}},\\
&\varepsilon_{18} = -\rho^2 - \varrho^2 + \frac{625\rho^2\varepsilon_{22}^2}{\varepsilon_{10}^2} + \frac{\varrho^2\varepsilon_{21}^2}{3\varepsilon_{11}} + \frac{3\varepsilon_{10}^3}{25}.
\end{aligned}
\tag{8}
$$

Substituting Eqs. (7) and (8) into Eq. (2), the three-order rogue wave solution of Eq. (1) is obtained as follows:

$$\kappa = x + \eta z - \Theta(t), \quad u = 2\,[\ln\psi]_{\kappa\kappa}, \quad \psi = \psi(\kappa, y), \tag{9}$$

When $\theta_3 = \theta_4 = \theta_6 = \theta_2 = 1$ in Eq. (9), we can see the interaction between three rogue waves in Figure 4. When $\theta_3 = \theta_6 = \theta_2 = 1$, $\theta_4 = t$ in Eq. (9), we can see the interaction between five rogue waves in Figure 5.

4 Six-order rogue wave solution

To present the six-order rogue wave solution of Eq. (1), we have

$$
\begin{aligned}
\psi(\kappa, y) = {} & \kappa^{12} + y^8\varepsilon_{48} + y^6\varepsilon_{47} + y^4\varepsilon_{46} + (\rho^2 + \varrho^2)(\kappa^2\\
& + y^2\varepsilon_1 + \varepsilon_0) + \varepsilon_{51} + \kappa^{10}(y^2\varepsilon_{26} + \varepsilon_{25}) + y^2\varepsilon_{45}\\
& + \kappa^8(y^4\varepsilon_{29} + y^2\varepsilon_{28} + \varepsilon_{27}) + y^{12}\varepsilon_{50} + y^{10}\varepsilon_{49}\\
& + 2\rho\kappa[\kappa^6 + y^6\varepsilon_{64} + y^4\varepsilon_{63} + \kappa^4(y^2\varepsilon_{69} + \varepsilon_{68})\\
& + y^2\varepsilon_{62} + \kappa^2(y^4\varepsilon_{67} + y^2\varepsilon_{66} + \varepsilon_{65}) + \varepsilon_{61}]\\
& + 2\varrho y[y^6 + y^4(\kappa^2\varepsilon_{57} + \varepsilon_{56}) + y^2(\kappa^4\varepsilon_{55}\\
& + \kappa^2\varepsilon_{54} + \varepsilon_{53}) + \kappa^6\varepsilon_{60} + \kappa^4\varepsilon_{59} + \kappa^2\varepsilon_{58} + \varepsilon_{52}]\\
& + \kappa^6[y^6\varepsilon_{33} + y^4\varepsilon_{32} + y^2\varepsilon_{31} + \varepsilon_{30}]\\
& + \kappa^4[y^8\varepsilon_{38} + y^6\varepsilon_{37} + y^4\varepsilon_{36} + y^2\varepsilon_{35} + \varepsilon_{34}]\\
& + \kappa^2(y^{10}\varepsilon_{44} + y^8\varepsilon_{43} + y^6\varepsilon_{42} + y^4\varepsilon_{41}\\
& + y^2\varepsilon_{40} + \varepsilon_{39}),
\end{aligned}
\tag{10}
$$

where ε_i $(i = 25, \ldots, 69)$ is undetermined constant. Substituting Eq. (10) into Eq. (3), we obtain

$$
\begin{aligned}
&\Theta(t) = \frac{1}{6}\int [6\theta_3 + 6\eta\theta_4 - \varepsilon_{26}\theta_5 + 6\eta^2\theta_6]\mathrm{d}t, \theta_2 = -\frac{\varepsilon_{26}^4\varepsilon_{59}\theta_5}{136080},\\
&\varepsilon_{32} = \frac{11\varepsilon_{26}^5\varepsilon_{59}}{5832}, \varepsilon_{31} = \frac{19\varepsilon_{26}^7\varepsilon_{59}^2}{3149280}, \varepsilon_{37} = \frac{73\varepsilon_{26}^6\varepsilon_{59}}{244944},\\
&\varepsilon_{36} = \frac{107\varepsilon_{26}^8\varepsilon_{59}^2}{52907904},\\
&\varepsilon_{45} = \varepsilon_1(-\rho^2 - \varrho^2) + \frac{\rho^2\varepsilon_{26}}{6} + \frac{46656\varrho^2}{\varepsilon_{26}^6}\\
&\qquad + \frac{3509\varepsilon_{59}^5\varepsilon_{26}^{16}}{1259660837552947200}, \varepsilon_{42} = \frac{253\varepsilon_{26}^9\varepsilon_{59}^2}{793618560},\\
&\varepsilon_{41} = -\frac{\varepsilon_{26}^{11}\varepsilon_{59}^3}{28570268160}, \varepsilon_{52} = \frac{11\varepsilon_{26}^6\varepsilon_{59}^3}{94478400}, \varepsilon_{33} = \frac{5\varepsilon_{26}^3}{54},\\
&\varepsilon_{55} = \frac{-180}{\varepsilon_{26}^2}, \varepsilon_{38} = \frac{5\varepsilon_{26}^4}{432}, \varepsilon_{35} = \frac{\varepsilon_{26}^{10}\varepsilon_{59}^3}{317447424},\\
&\varepsilon_{43} = \frac{19\varepsilon_{26}^7\varepsilon_{59}}{979776}, \varepsilon_{29} = \frac{5\varepsilon_{26}^2}{12},
\end{aligned}
$$

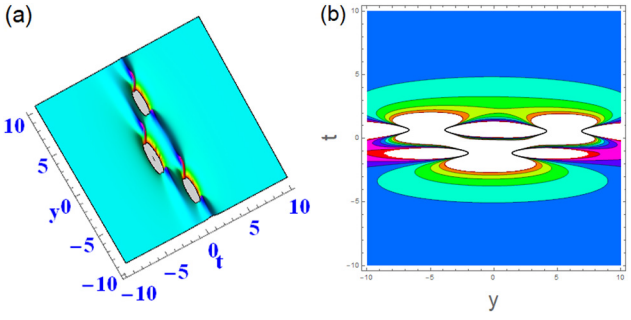

Figure 4: $\eta = -1, \varepsilon_{10} = -6, \varepsilon_{11} = \varepsilon_{21} = \varepsilon_{22} = 1, \rho = \varrho = 10, x = z = 0$, (a) 3D plot and (b) contour plot.

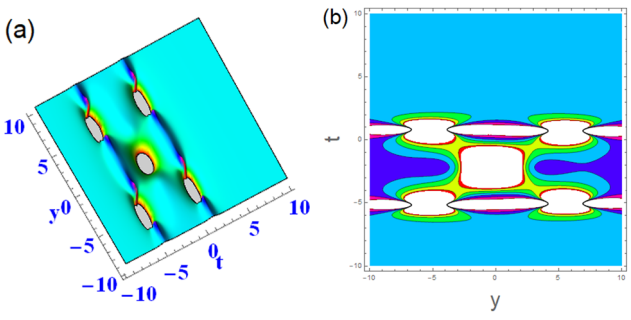

Figure 5: $\eta = -1, \varepsilon_{10} = -6, \varepsilon_{11} = \varepsilon_{21} = \varepsilon_{22} = 1, \rho = \varrho = 10, x = z = 0$, (a) 3D plot and (b) contour plot.

$$\varepsilon_{50}=\frac{\varepsilon_{26}^{6}}{46656},\ \varepsilon_{54}=\frac{-19}{63}\varepsilon_{26}\varepsilon_{59},\ \varepsilon_{57}=\frac{-54}{\varepsilon_{26}},$$
$$\varepsilon_{49}=\frac{29\varepsilon_{26}^{8}\varepsilon_{59}}{88179840},\ \varepsilon_{63}=\frac{\varepsilon_{26}^{5}\varepsilon_{59}}{18144},\ \varepsilon_{48}=\frac{289\varepsilon_{26}^{10}\varepsilon_{59}^{2}}{44442639360},$$
$$\varepsilon_{40}=\frac{11\varepsilon_{26}^{13}\varepsilon_{59}^{4}}{30855889612800},\ \varepsilon_{61}=\frac{7\varepsilon_{26}^{9}\varepsilon_{59}^{3}}{20407334400},$$
$$\varepsilon_{64}=\frac{5\varepsilon_{26}^{3}}{216},\ \varepsilon_{47}=\frac{5707\varepsilon_{26}^{12}\varepsilon_{59}^{3}}{53997806822400},\ \varepsilon_{27}=\frac{\varepsilon_{26}^{6}\varepsilon_{59}^{2}}{699840},$$
$$\varepsilon_{66}=\frac{-23\varepsilon_{26}^{4}\varepsilon_{59}}{13608},\ \varepsilon_{53}=\frac{-\varepsilon_{26}^{4}\varepsilon_{59}^{2}}{58320},\ \varepsilon_{60}=\frac{1080}{\varepsilon_{26}^{3}},$$
$$\varepsilon_{69}=\frac{3\varepsilon_{26}}{-2},\ \varepsilon_{65}=\frac{\varepsilon_{26}^{6}\varepsilon_{59}^{2}}{-2099520},\ \varepsilon_{28}=\frac{23\varepsilon_{26}^{4}\varepsilon_{59}}{4536},$$
$$\varepsilon_{25}=\frac{7\varepsilon_{26}^{3}\varepsilon_{59}}{1620},\ \varepsilon_{56}=\frac{-1}{540}\varepsilon_{26}^{2}\varepsilon_{59},$$
$$\varepsilon_{46}=\frac{13381\varepsilon_{26}^{14}\varepsilon_{59}^{4}}{23327052547276800},\ \varepsilon_{67}=\frac{5\varepsilon_{26}^{2}}{-36},$$
$$\varepsilon_{34}=\frac{-121\varepsilon_{26}^{12}\varepsilon_{59}^{4}}{18513533767680},\ \varepsilon_{68}=\frac{13\varepsilon_{26}^{3}\varepsilon_{59}}{22680},$$
$$\varepsilon_{58}=\frac{19\varepsilon_{26}^{3}\varepsilon_{59}^{2}}{-68040},\ \varepsilon_{44}=\frac{\varepsilon_{26}^{5}}{1296},\ \varepsilon_{30}=\frac{11\varepsilon_{26}^{9}\varepsilon_{59}^{3}}{5101833600},$$
$$\varepsilon_{39}=-\varrho^{2}+\frac{279936\varrho^{2}}{\varepsilon_{26}^{7}}+\frac{1331\varepsilon_{59}^{5}\varepsilon_{26}^{15}}{149959623518208000},$$
$$\varepsilon_{62}=\frac{107\varepsilon_{26}^{7}\varepsilon_{59}^{2}}{617258880},\ \varepsilon_{51}=\varepsilon_{0}(-\rho^{2}-\varrho^{2})+\frac{\varepsilon_{59}(279936\varrho^{2}+\rho^{2}\varepsilon_{26}^{7})}{7560\varepsilon_{26}^{4}}+\frac{14641\varepsilon_{59}^{6}\varepsilon_{26}^{18}}{20406505568357744640000},\quad(11)$$
$$\varrho(t)=-\frac{136080\beta(t)}{\varepsilon_{26}^{4}\varepsilon_{59}},\ \theta_{7}=0.$$

Substituting Eqs. (10) and (11) into Eq. (2), the six-order rogue wave solution of Eq. (1) is obtained as follows:

$$\kappa=x+\eta z-\Theta(t),\quad u=2\,[\ln\psi]_{\kappa\kappa},\quad \psi=\psi(\kappa,y).\quad(12)$$

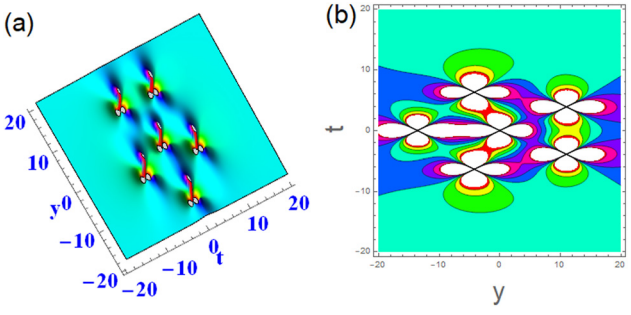

Figure 6: $\eta=-1$, $\varepsilon_0=-2$, $\varepsilon_1=\varepsilon_{59}=\varepsilon_{26}=1$, $\rho=\varrho=10$, $x=z=0$, (a) 3D plot and (b) contour plot.

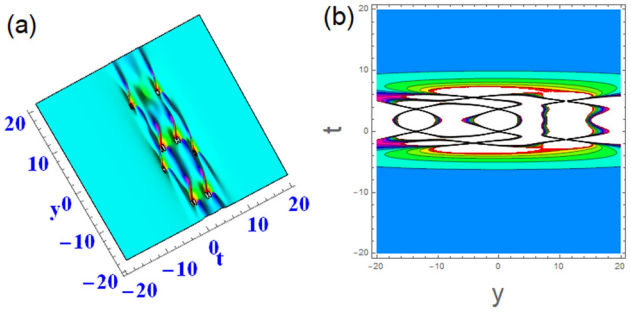

Figure 7: $\eta=-1$, $\varepsilon_0=-2$, $\varepsilon_1=\varepsilon_{59}=\varepsilon_{26}=1$, $\rho=\varrho=10$, $x=z=0$, (a) 3D plot and (b) contour plot.

When $\theta_3=\theta_4=\theta_6=\theta_2=1$ in Eq. (12), we can see the interaction between six rogue waves in Figure 6. When $\theta_3=\theta_6=\theta_2=1$, $\theta_4=t$ in Eq. (12), we can see the interaction between eight rogue waves in Figure 7.

5 Conclusion

In this work, a generalized (3+1)-dimensional vcKPe are studied. Based on the modified symbolic computation approach and symbolic computation [16–44], we obtain the multiple rogue wave solutions of the generalized (3+1)-dimensional vcKPe. By selecting different functions of the variable coefficient, the dynamic properties of the derived solutions are shown in Figures 1–7. In Figure 1, we can find a rogue wave spreading. When $\theta_4=t$, two rogue waves can be seen in Figure 2. When θ_4 and θ_6 are selected as trigonometric functions, a periodic-type rogue wave is shown in Figure 3. In Figure 4, we can observe the interaction between three rogue waves. The interaction between five rogue waves is shown in Figure 5. Further, the interaction between six rogue waves is shown in Figure 6, and the interaction between eight rogue waves is shown in Figure 7.

Funding information: The authors state no funding involved.

Author contributions: All authors have accepted responsibility for the entire content of this manuscript and approved its submission.

Conflict of interest: The authors state no conflict of interest.

Data availability statement: Data sharing not applicable to this article as no datasets were generated or analyzed during the current study.

References

[1] Deng YF, Yang JM, Li X, Xiao LF. A review on the freak wave generation in the wave tank. J Ship Mech. 2016;20(8):1059–70.

[2] Draper L. Freak wave. Marine Observer. 1965;35(2):193.

[3] Tukur AS, Abdullahi Y, Alrazi A, Marwan A. Dynamics of lump collision phenomena to the (3+1)-dimensional nonlinear evolution equation. J Geom Phys. 2021;169:104347.

[4] Tukur AS, Abdullahi Y. Dynamics of lump-periodic and breather waves solutions with variable coefficients in liquid with gas bubbles. Wave Random Complex. 2021. doi: 10.1080/17455030.2021.1897708.

[5] Abdullahi Y, Tukur AS. Dynamics of Lump-periodic, breather and two-wave solutions with the long wave in shallow water under gravity and 2D nonlinear lattice. Commun Nonlinear Sci. 2021;99:105846.

[6] Jaradat HM, Shara SA, Awawdeh F, Alquran M. Variable coefficient equationsof the Kadomtsev–Petviashvili hierarchy: multiple soliton solutions and singular multiplesoliton solutions. Phys Scr. 2012;85(3):035001.

[7] Xie XY, Tian B, Jiang Y, Zhong H, Sun Y, Wang YP. Painlevé analysis, soliton collision and Bäcklund transformation for the (3+1)-dimensional variable-coefficient Kadomtsev–Petviashvili equation in fluids or plasmas. Commun Theor Phys. 2014;62:26–32.

[8] Chai J, Tian B, Sun WR, Xie XY. Solitons and rouge waves for a generalized (3+1)-dimensional variable-coefficient Kadomtsev–Petviashvili equation in fluid mechanics. Comput Math Appl. 2016;71:2060–8.

[9] Yin Y, Tian B, Chai HP, Yuan YQ, Du Z. Lumps and rouge waves for a (3+1)-dimensional variable-coefficient Kadomtsev–Petviashvili equation in fluid mechanics. Pramana-J Phys. 2018;91:43.

[10] Chai J, Tian B, Wu XY, Liu L. Fusion and fission phenomena for the soliton interactions in a plasma. Eur Phys J Plus. 2017;132:60.

[11] Chen SS, Tian B. Gramian solutions and soliton interactions for a generalized (3+1)-dimensional variable-coefficient Kadomtsev–Petviashvili equation in a plasma or fluid. Proc R Soc A. 2019;475:20190122.

[12] Liu JG, Zhu WH. Various exact analytical solutions of a variable-coefficient Kadomtsev–Petviashvili equation. Nonlinear Dyn. 2020;100:2739–51.

[13] Liu JG, Zhu WH. Multiple rogue wave, breather wave and interaction solutions of a generalized (3+1)-dimensional variable-coefficient nonlinear wave equation. Nonlinear Dyn. 2021;103:1841–50.

[14] Liu JG, Zhu WH. Multiple rogue wave solutions for (2+1)-dimensional Boussinesq equation. Chinese J Phys. 2020;67:492–500.

[15] Liu JG, Zhu WH, He Y. Variable-coefficient symbolic computation approach for finding multiple rogue wave solutions of nonlinear system with variable coefficients. Z Angew Math Phys. 2021;72:154.

[16] Ma WX. N-soliton solution of a combined pKP-BKP equation. J Geom Phys. 2021;165:104191.

[17] Zhang RF, Li MC, Albishari M, Zheng FC, Lan ZZ. Generalized lump solutions, classical lump solutions and rogue waves of the (2+1)-dimensional Caudrey-Dodd-Gibbon-Kotera-Sawada-like equation. Appl Math Comput. 2021;403:126201.

[18] Ma WX, Yong XL, Lü X. Soliton solutions to the B-type Kadomtsev–Petviashvili equation under general dispersion relations. Wave Motion. 2021;103:102719.

[19] Liu JG, Zhu WH, Zhou L. Breather wave solutions for the Kadomtsev–Petviashvili equation with variable coefficients in a fluid based on the variable-coefficient three-wave approach. Math Method Appl Sci. 2020;43(1):458–65.

[20] Liu JG, Osman MS, Zhu WH, Zhou L, Ai GP. Different complex wave structures described by the Hirota equation with variable coefficients in inhomogeneous optical fibers. Appl Phys B-Lasers O. 2019;125:175.

[21] Baronio F, Conforti M, Degasperis A, Lombardo S. Rogue waves emerging from the resonant interaction of three waves. Phys Rev Lett. 2013;111:114101.

[22] Marwan A, Tukur AS, Abdullahi Y. Kink-soliton, singular-kink-soliton and singular-periodic solutions for a new two-mode version of the Burger-Huxley model: applications in nerve fibers and liquid crystals. Opt Quant Electron. 2021;53:227.

[23] Wang L, Luan Z, Zhou Q, Anjan B, Abdullah KA, Liu W. Bright soliton solutions of the (2+1)-dimensional generalized coupled nonlinear Schrödinger equation with the four-wave mixing term. Nonlinear Dyn. 2021;104(3):2613–20.

[24] Tukur AS, Abdullahi Y, Fairouz T, Mustafa I, Tawfiq FMO, Bousbahi F. Lie-Bäcklund symmetries, analytical solutions and conservation laws to the more general (2+1)-dimensional Boussinesq equation. Results Phys. 2021;22:103850.

[25] Liu X, Zhang H, Liu W. The dynamic characteristics of pure-quartic solitons and soliton molecules. Appl Math Model. 2022;102:305–12.

[26] Haci MB, Tukur AS, Hasan B. On the exact solitary wave solutions to the long-short wave interaction system. ITM Web Confer. 2018;22:01063.

[27] Liu JG, Zhu WH, Osman MS, Ma WX. An explicit plethora of different classes of interactive lump solutions for an extension form of 3D-Jimbo-Miwa model. Eur Phys J Plus. 2020;135(5):412.

[28] Zhou Q, Wang T, Anjan B, Liu W. Nonlinear control of logic structure of all-optical logic devices using soliton interactions. Nonlinear Dyn. 2022;107:1215–22.

[29] Neslihan O, Handenur E, Aydin S, Mustafa B, Tukur AS, Abdullahi Y, et al. Optical solitons and other solutions to the Radhakrishnan-Kundu-Lakshmanan equation. Optik. 2021;242:167363.

[30] Zhou Q. Influence of parameters of optical fibers on optical soliton interactions. Chin Phys Lett. 2022;39(1):010501.

[31] Ali KK, Wazwaz AM, Osman MS. Optical soliton solutions to the generalized nonautonomous nonlinear Schrödinger equations in optical fibers via the sine-Gordon expansion method. Optik. 2020;208:164132.

[32] Osman MS. Multiwave solutions of time-fractional (2+1)-dimensional Nizhnik-Novikov-Veselov equations. Pramana-J Phys. 2017;88(4):67.

[33] Yan YY, Liu WJ. Soliton rectangular pulses and bound states in a dissipative system modeled by the variable-coefficients complex cubic-quintic Ginzburg-Landau equation. Chin Phys Lett. 2021;38(9):094201.

[34] Osman MS. Multi-soliton rational solutions for some nonlinear evolution equations. Open Phys. 2016;14:26–36.
[35] Ouyang Y, You T, Zhou Q, Liu M, Hou H, Liu X, et al. Layered AuTe2Se4/3 for a stable nanosecond Q-switched fiber laser. Optik. 2020;204:164231.
[36] Abdel-Gawad HI, Osman MS. Exact solutions of the Korteweg-de Vries equation with space and time dependent coefficients by the extended unified method. Indian J Pure Ap Math. 2014;45(1):1–11.
[37] Ali KK, Osman MS, Mahmoud AA. New optical solitary wave solutions of Fokas-Lenells equation in optical fiber via Sine-Gordon expansion method. Alex Eng J. 2020;59(3):1191–6.
[38] Haci MB, Hasan B, Tukur AS. Investigation of various travelling wave solutions to the extended (2+1)-dimensional quantum ZK equation. Eur Phys J Plus. 2017;132:482.
[39] Sunil K, Ranbir K, Osman MS, Bessem S. A wavelet based numerical scheme for fractional order SEIR epidemic of measles by using Genocchi polynomials. Numer Meth Part D E. 2021;37(2):1250–68.
[40] Bilge I, Osman MS, Turgut A, Dumitru B. Analytical and numerical solutions of mathematical biology models: The Newell-Whitehead-Segel and Allen-Cahn equations. Math Method Appl Sci. 2020;43(5):2588–600.
[41] Zhao J, Luan Z, Zhang P, Dai C, Anjan B, Liu W, et al. Dark three-soliton for a nonlinear Schrödinger equation in inhomogeneous optical fiber. Optik. 2020;220:165189.
[42] Aasma K, Akmal R, Kottakkaran SN, Osman MS. Splines solutions of boundary value problems that arises in sculpturing electrical process of motors with two rotating mechanism circuit. Phys Scripta. 2021;96(10):104001.
[43] Osman MS, Machado JAT, Dumitru B. On nonautonomous complex wave solutions described by the coupled Schrödinger-Boussinesq equation with variable-coefficients. Opt Quant Electron. 2018;50(2):73.
[44] Haci MB, Osman MS, Hamood R, Muhammad R, Muhammad T, Shagufta A. On pulse propagation of soliton wave solutions related to the perturbed Chen-Lee-Liu equation in an optical fiber. Opt Quant Electron. 2021;53(10):556.